

DMIS: Dynamic Mesh-based Importance Sampling for Training Physics-Informed Neural Networks

Zijiang Yang,^{1,2} Zhongwei Qiu,^{1,2,3} Dongmei Fu^{1,2,4}

¹School of Automation and Electrical Engineering, University of Science and Technology Beijing

²Beijing Engineering Research Center of Industrial Spectrum Imaging

³The University of Sydney

⁴Shunde Innovation School, University of Science and Technology Beijing

zijiayang@xs.ustb.edu.cn, qiuzhongwei@xs.ustb.edu.cn, fdm_ustb@ustb.edu.cn

Abstract

Modeling dynamics in the form of partial differential equations (PDEs) is an effectual way to understand real-world physics processes. For complex physics systems, analytical solutions are not available and numerical solutions are widely-used. However, traditional numerical algorithms are computationally expensive and challenging in handling multiphysics systems. Recently, using neural networks to solve PDEs has made significant progress, called physics-informed neural networks (PINNs). PINNs encode physical laws into neural networks and learn the continuous solutions of PDEs. For the training of PINNs, existing methods suffer from the problems of inefficiency and unstable convergence, since the PDE residuals require calculating automatic differentiation. In this paper, we propose **Dynamic Mesh-based Importance Sampling (DMIS)** to tackle these problems. DMIS is a novel sampling scheme based on importance sampling, which constructs a dynamic triangular mesh to estimate sample weights efficiently. DMIS has broad applicability and can be easily integrated into existing methods. The evaluation of DMIS on three widely-used benchmarks shows that DMIS improves the convergence speed and accuracy in the meantime. Especially in solving the highly nonlinear Schrödinger Equation, compared with state-of-the-art methods, DMIS shows up to 46% smaller root mean square error and five times faster convergence speed. Code is available at <https://github.com/MatrixBrain/DMIS>.

Introduction

Modeling the dynamics of real-world physics systems has important guiding significance for production activities, such as fluid mechanics and heat transfer. These physics systems are usually described by partial differential equations (PDEs). Due to the highly nonlinear of these PDEs, in most cases, analytical solutions are not available.

In the past decades, numerical algorithms for solving PDEs have been greatly developed. Although classical numerical algorithms significantly promoted the development of related fields, these algorithms are computationally expensive and face severe challenges in multiphysics and multiscale systems. With the improvement of data acquisition capability, it is an important issue to use data to modify simulation results. In general, data assimilation is the primary method to combine classical numerical algorithms and observation data, but data assimilation introduces additional

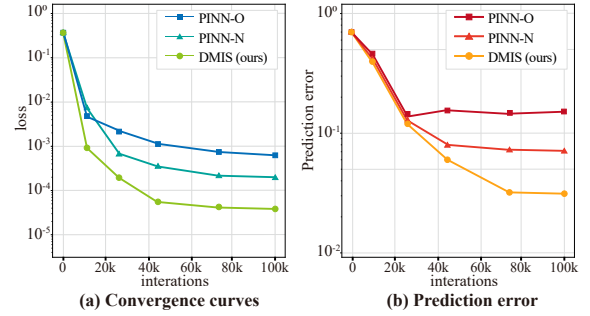


Figure 1: Comparison with state-of-the-art methods (PINN-O, PINN-N). DMIS achieves faster convergence speed and better prediction accuracy.

uncertainties and seriously affects convergence.

Recently, with the rapid development of machine learning, the ability to extract features and mine information from observation data has been dramatically improved. (Krizhevsky, Sutskever, and Hinton 2012; He et al. 2016). As an effective supplement to classical numerical methods, Physics-informed Neural Networks (PINNs) formulate the problem of solving PDEs into a parameter optimization problem (Raissi, Perdikaris, and Karniadakis 2019). PINNs encode PDEs into the loss function of neural networks. In addition, boundary conditions and initial conditions are also integrated into the loss function as soft constraints. PINNs are mesh-free and learn continuous solutions of PDEs. Practices show that PINNs can be applied to solve different types of PDEs (Raissi, Perdikaris, and Karniadakis 2019; Pang, Lu, and Karniadakis 2019; Zhang, Guo, and Karniadakis 2020). Since partial derivative terms of PDE residuals require automatic differentiation to calculate, the training of PINNs is computationally expensive and unstable. Especially for solving PDEs with high order partial derivative terms, these defects are more prominent. Therefore, in the studies of PINNs, it is a critical issue to design schemes to stabilize training and improve training efficiency.

Three mainstream improvement directions are deeply studied for the training of PINNs, including weights of loss terms, parallel computation, and sampling. The loss function of PINNs contains multiple loss terms, and methods of weight allocation are mainly to balance these terms. These

methods usually need to be customized according to physics systems, which limits the applications. The efficient parallel computation of PINNs can be realized by decomposing the whole domain into several subdomains. Nevertheless, domain decomposition involves additional subdomain boundary conditions and affects the convergence efficiency and model accuracy. The last mainstream improvement direction, sampling, improves training efficiency and model accuracy by changing the sampling probability of data. Due to broad applicability, it attracts increasing attention.

The training of PINNs involves two sampling processes. The first sampling process is to build a training dataset from the whole domain, and the second is to sample mini-batch data in each iteration for parameter optimization. In order to distinguish, in this paper, we refer to the first sampling process as generating collocation points. Currently, the progress in sampling mainly focuses on the generation of collocation points. These collocation points generation approaches improve the training efficiency by constructing a better training dataset without incurring additional computational costs. The mini-batch sampling significantly impacts convergence speed and model accuracy, which has been verified in other fields (Shrivastava, Gupta, and Girshick 2016; Kang et al. 2019; Mildenhall et al. 2020; Lei et al. 2021). However, the mini-batch sampling for PINNs has not been fully studied. In uniform sampling, the training spends most of computation on data points that are not helpful for optimization.

In our previous research, we found that training efficiency and model accuracy can be improved by introducing well-designed weighting algorithm in other fields (Qiu et al. 2019, 2020; Wang et al. 2021; Qiu et al. 2022). In this paper, we introduce additional weighting algorithm and propose a novel sampling scheme, called Dynamic Mesh-based Importance Sampling (DMIS), to speed up the training of PINNs. To guarantee the sampling method theoretically, we introduce the concept of importance sampling into DMIS. However, importance sampling requires calculating the sampling probability of each point, which leads to high computational costs. To reduce the computational cost, we propose a novel sampling weight estimation method, called Dynamic Mesh-based weight estimation (DMWE), which constructs a dynamic triangular mesh to estimate the weight of each data point efficiently. The mesh constructed by DMWE is updated dynamically according to the loss distribution in the whole domain during training. DMIS efficiently integrates importance sampling into the training of PINNs, and has a low computational cost and broad applicability. As shown in Figure 1, DMIS achieves faster convergence speed and better accuracy compared with the state-of-the-art methods.

Our contributions can be summarized as follows:

- We propose an efficient importance sampling scheme for training PINNs, which improves the training convergence speed and the model accuracy without significantly increasing computational cost.
- We propose a method to calculate sample weights in PINNs efficiently. In addition to be used in our importance sampling scheme, this method is also suitable for other approaches that need to calculate sample weights.

- The extensive experiments on three widely-used benchmarks demonstrate the superior performance of our importance sampling scheme.

Related Work

Physics-Informed Neural Networks In recent years, benefited from the significant progress of deep learning, the method of solving PDEs based on neural networks has been dramatically developed. According to the method of embedding physics laws, all of these methods based on neural networks for solving PDEs can be grouped into three types, including observational bias (Umetani and Bickel 2018), inductive bias (Cai, Li, and Liu 2020; Dong and Ni 2021) and learning bias (Sirignano and Spiliopoulos 2018; Raissi, Perdikaris, and Karniadakis 2019). Among these methods, physics-informed neural networks attract increasing attention, owing to excellent augment ability (Niaki et al. 2021; Raissi, Yazdani, and Karniadakis 2020; Wandel et al. 2022).

The training of PINNs is computationally expensive and unstable. To alleviate these defects of PINNs, allocation of loss weights (Wang, Teng, and Perdikaris 2021; Wang, Yu, and Perdikaris 2022; Krishnapriyan et al. 2021), parallel computation methods (Meng et al. 2020; Jagtap and Karniadakis 2020) and sampling schemes (Lu et al. 2021; Nabian, Gladstone, and Meidani 2021; Daw et al. 2022; Wu et al. 2022) have been widely discussed and improve the convergence efficiency and prediction accuracy of PINNs. Gradient control methods are also studied (Kim et al. 2021).

Importance Sampling Importance sampling is an effective method to accelerate Monte Carlo Integration, which has been applied to train neural networks (Schaul et al. 2015; Chen, Ma, and Xiao 2018; Meng et al. 2022). It has been proved theoretically that the SGD has the fastest convergence speed if the mini-batch is sampled according to a unique distribution that the sampling probability of each point is proportional to the 2-norm of loss gradient with respect to parameters (Needell, Ward, and Srebro 2014; Zhao and Zhang 2015). The computational cost of the theoretical optimal method is prohibitive. Follow-up works mainly focus on finding approximation methods (Loshchilov and Hutter 2015; Canévet, Jose, and Fleuret 2016; Johnson and Guestrin 2018; Katharopoulos and Fleuret 2018). To our best knowledge, only Nabian, Gladstone, and Meidani (2021) preliminary explores the combination of importance sampling and the training of PINNs.

Optimization Problem of PINNs

PINNs learn an approximate solution $\hat{u}(t, \mathbf{x}; \boldsymbol{\theta})$ to fit the latent solution $u(t, \mathbf{x})$ of the following PDE:

$$\begin{aligned} \frac{\partial u}{\partial t} + \mathcal{N}_{\mathbf{x}}[u] &= 0, \mathbf{x} \in \Omega, t \in [0, T], \\ u(t, \mathbf{x})|_{t=0} &= u_0(\mathbf{x}), \mathbf{x} \in \Omega, \\ u(t, \mathbf{x}) &= g(t, \mathbf{x}), \mathbf{x} \in \partial\Omega, t \in [0, T], \end{aligned} \quad (1)$$

where $\boldsymbol{\theta}$ is the parameter of PINNs, $\mathcal{N}_{\mathbf{x}}$ denotes a differential operator consisted of spatial derivatives, $u_0(\mathbf{x})$ is the

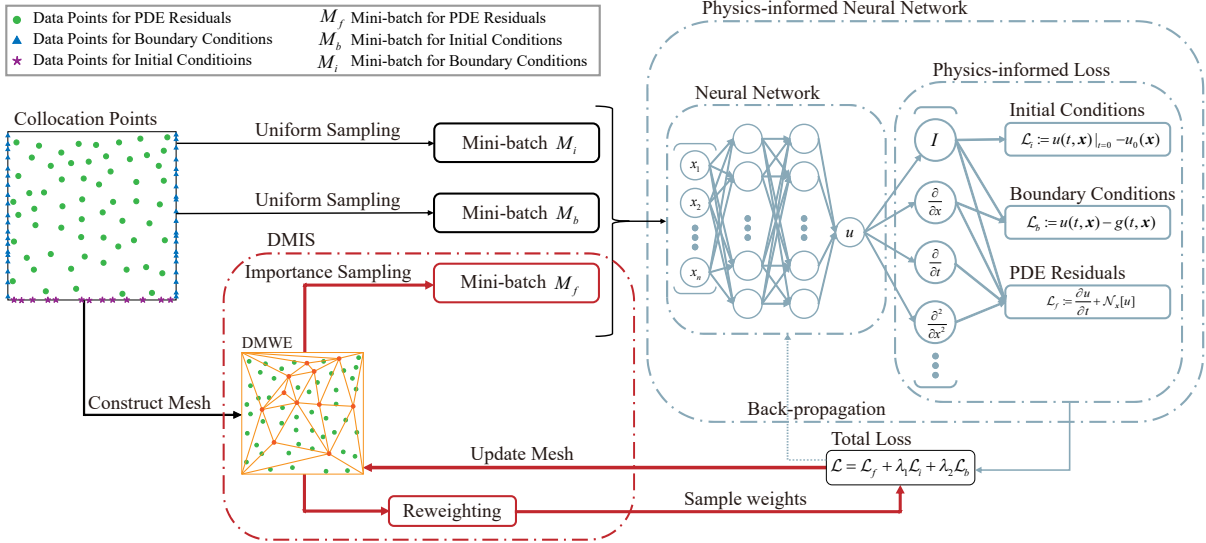


Figure 2: The Training of PINNs with DMIS. In each iteration, sample weights are estimated by DMWE, and a mini-batch for PDE residuals is sampled by DMIS. The derivatives terms are computed by automatic differentiation. These mini-batches are applied to compute the initial conditions loss \mathcal{L}_i , boundary conditions loss \mathcal{L}_b , and PDE residuals loss \mathcal{L}_f . DMIS reweights sample weights of M_f and conveys these weights to the loss function \mathcal{L} . The mesh of DMIS is updated according to \mathcal{L} .

initial condition, $g(\mathbf{x})$ is the boundary condition, \mathbf{x} is a D -dimensional position vector, and Ω is a subset of \mathbb{R}^D with boundary $\partial\Omega$. For the convenience of subsequent discussion, the input vector composed of time t and space vector \mathbf{x} is denoted as \mathbf{x} . The optimization goal of PINNs is to minimize the residual of PDEs with the constraints of satisfying boundary conditions and initial conditions:

$$\begin{aligned} \boldsymbol{\theta}^* &= \arg \min_{\boldsymbol{\theta}} r_f(\boldsymbol{\theta}), \\ \text{s.t. } r_i(\boldsymbol{\theta}) &= 0, r_b(\boldsymbol{\theta}) = 0, \end{aligned} \quad (2)$$

where $r_f(\boldsymbol{\theta})$, $r_i(\boldsymbol{\theta})$ and $r_b(\boldsymbol{\theta})$ are the residuals of PDEs, initial conditions, and boundary conditions, respectively.

Equation (2) is difficult to solve. PINNs regard constraints as penalty terms and formulate the constrained optimization problem into an unconstrained optimization problem:

$$\boldsymbol{\theta}^* = \arg \min_{\boldsymbol{\theta}} r_f(\boldsymbol{\theta}) + \lambda_1 r_i(\boldsymbol{\theta}) + \lambda_2 r_b(\boldsymbol{\theta}), \quad (3)$$

where λ_1 and λ_2 are weights. The common practice of PINNs is to fit $\boldsymbol{\theta}$ by Monte Carlo approximation. PINNs generate collocation points from spatial-temporal domains uniformly, and mini-batch stochastic gradient descent method (SGD) is employed to optimize parameters. Focusing on data points helpful for parameter optimization is a more efficient sampling strategy. Monte-Carlo approximation has provided the mathematical tools, called importance sampling, to design such a sampling method.

Method

Sampling approaches significantly impact training efficiency. Recent works mainly focus on the generation of collocation points, while the mini-batch sampling is neglected. Motivated by the theoretical completeness of importance

sampling and the non-negligible impact of mini-batch sampling, we design a novel sampling approach for mini-batch sampling based on importance sampling to improve the convergence speed and model accuracy of PINNs.

Importance Sampling for PINNs PINNs generate collocation points from domain and domain boundary. Equation (3) can be approximated as a loss function of data points:

$$\boldsymbol{\theta}^* \approx \arg \min_{\boldsymbol{\theta}} \mathcal{L}_f + \lambda_1 \mathcal{L}_i + \lambda_2 \mathcal{L}_b, \quad (4)$$

where \mathcal{L}_f , \mathcal{L}_i , and \mathcal{L}_b are the losses of PDE residuals, initial conditions, and boundary conditions, respectively.

Datasets for PDE residuals, initial conditions and boundary conditions are denoted by N_f , N_i and N_b , respectively. In general, mini-batches are uniformly sampled from N_f , N_i , and N_b , respectively. According to the Monte Carlo approximation, we can introduce a more efficient sampling method. Because boundary conditions and initial conditions are penalty terms, we only introduce importance sampling into the sampling of N_f . The loss of PDE residuals \mathcal{L}_f combined with importance sampling is shown as:

$$\mathcal{L}_f = \frac{1}{|N_f|} \sum_{i=1}^{|N_f|} \alpha_i \ell_f(x_i; \boldsymbol{\theta}), \quad \alpha_i = \frac{p_i}{q_i}, \quad (5)$$

where $|N_f|$ is the size of N_f , ℓ_f is the PDE residual of each data point, α_i , p_i and q_i are sample weight, sampling probability and alternative sampling probability of data point x_i , respectively. Considering mini-batches are obtained by uniform sampling in general, p_i equals to $1/|N_f|$ for $i \in \{1, 2, \dots, |N_f|\}$ and the calculation of α_i is shown as:

$$\alpha_i = \frac{1}{|N_f| q_i}, \quad i \in \{1, 2, \dots, |N_f|\}, \quad (6)$$

Simplified Calculation & Reweighting The critical issue of importance sampling is to determine q_i for $i \in \{1, 2, \dots, |N_f|\}$ and we hope to find the best alternative sampling distribution to make the convergence rate fastest. Suppose convergence rate is defined as:

$$C^{(t)} = -\mathbb{E}_f[\|\boldsymbol{\theta}^{(t+1)} - \boldsymbol{\theta}^*\|_2^2 - \|\boldsymbol{\theta}^{(t)} - \boldsymbol{\theta}^*\|_2^2], \quad (7)$$

where $C^{(t)}$ is the convergence rate at step t , $\boldsymbol{\theta}^{(t)}$ and $\boldsymbol{\theta}^{(t+1)}$ are parameters at step t and $t + 1$, respectively.

With the definition of convergence rate shown in Equation (7), [Needell, Ward, and Srebro \(2014\)](#); [Zhao and Zhang \(2015\)](#) have demonstrated that the best sampling probability of collocation points is determined by $q^* \propto \|\nabla_{\boldsymbol{\theta}} \ell_f(\mathbf{x}, \boldsymbol{\theta})\|_2$.

However, the computational cost of this theoretical optimal sampling method is unacceptable, and it is necessary to find alternative methods. Inspired by [Katharopoulos and Fleuret \(2017\)](#), an approximation calculation of the theoretical optimal formula is employed in DMIS.

$$q_i^{(t)} = \frac{\ell_f(\mathbf{x}_i, \boldsymbol{\theta}^{(t)})}{\sum_{j=1}^{|N_f|} \ell_f(\mathbf{x}_j, \boldsymbol{\theta}^{(t)})}, \quad i \in \{1, 2, \dots, |N_f|\}, \quad (8)$$

where $q_i^{(t)}$ is the sampling probability of \mathbf{x}_i at step t . [Katharopoulos and Fleuret \(2017\)](#) also demonstrate that Equation (8) does not change the rank of sampling probability. $\forall i, j \in \{1, 2, \dots, |N_f|\}$, if $q_i^* < q_j^*$, we can obtain that $q_i^{(t)} < q_j^{(t)}$. Therefore, Equation (8) is a reasonable approximation. However, we find that sample weights calculated by Equation (8) lead to unstable training in the initial stage. This problem is caused by data points with high loss, which lead to sharp local gradients. To fix this problem, we introduce a super parameter β to adjust α . With $\beta > 1$, greater penalties are applied to data points with high loss and the result is denoted as α' :

$$\alpha'_i = \left(\frac{1}{|N_f|q_i}\right)^\beta, \quad \beta \in [1, +\infty), \quad i \in \{1, 2, \dots, |N_f|\}. \quad (9)$$

DMWE Since Equation (8) reduces the computational cost of each data point, the sampling probability still needs to be calculated point by point, and it is an enormous burden in solving complex PDEs. To further reduce the computational cost, we propose dynamic mesh-based weight estimation (DMWE) to calculate sample weight by interpolation.

In DMWE, interpolation based on Delaunay Triangulation is employed. Specifically, We dynamically generate a subset S from N_f to construct a triangular mesh. DMWE only calculated the sample weights of points in S exactly, and the weights of other points are obtained by interpolation. S is generated according to Equation (10).

$$g_i^{(t)} \propto \|q_i^{(t)} - q_i^{(t-1)}\|, \quad i \in \{1, 2, \dots, |N_f|\}, \quad (10)$$

where $g_i^{(t)}$ is the selection probability of point \mathbf{x}_i at step t . Equation (10) reduces the number of mesh points in the inactive region to reduce the computational cost. Meanwhile, Equation (10) also ensures high-precision interpolation in the active region.

Algorithm 1: Sampler with DMIS

Input: batch size of PDE residuals $|M_f|$.

Parameter: set size of mesh points $|S|$, reweighting parameter β , mesh update threshold γ , dataset of PDE residuals N_f , iteration step t .

Output: mini-batch M_f , vector of sample weights α' .

Initialization

- 1: $t_0 \leftarrow 0$
- 2: $q_i^{(t_0)} \leftarrow 1/|N_f|, i \in \{1, 2, \dots, |N_f|\}$
- 3: $g_i^{(t_0)} \leftarrow 1/|N_f|, i \in \{1, 2, \dots, |N_f|\}$
- 4: $S \leftarrow |S|$ points sampled with $g_i^{(t_0)}$ from N_f
- 5: Build triangular mesh by Delaunay Triangulation

Mini-batch Sampling

- 1: Compute $\{\ell_f(\mathbf{x}_i, \boldsymbol{\theta}^{(t-1)})\}_{\mathbf{x}_i \in S}$
 - 2: Estimate score of other points in N_f by interpolation
 - 3: Compute $q_i^{(t)}$ according to Equation (8)
 - 4: $M_f \leftarrow |M_f|$ points sampled with $q_i^{(t)}$ from N_f
 - 5: Compute $\alpha_i^{(t)}$ according to Equation (6)
 - 6: Compute $\alpha'_i{}^{(t)}$ according to Equation (9)
 - 7: Compute $\text{Sim}(\mathbf{v}^{(t_0)}, \mathbf{v}^{(t)})$ according to Equation (11)
 - 8: **if** $\text{Sim}(\mathbf{v}^{(t_0)}, \mathbf{v}^{(t)}) < \gamma$ **then**
 - 9: $g_i^{(t)} \propto \|q_i^{(t-1)} - q_i^{(t_0)}\|, i \in \{1, 2, \dots, |N_f|\}$
 - 10: $q_i^{(t_0)} \leftarrow q_i^{(t)}, i \in \{1, 2, \dots, |N_f|\}$
 - 11: $S \leftarrow |S|$ points sampled with g_i from N_f
 - 12: $t_0 \leftarrow t$
 - 13: Update mesh by Delaunay Triangulation
 - 14: **end if**
 - 15: **return** M_f, α'
-

The interpolation based on Delaunay is time-consuming and it is also unnecessary to update the triangular mesh in each iteration step. Therefore, we introduce the cosine similarity-based evaluation method to decide whether to re-select S and rebuild the triangular mesh.

$$\text{Sim}(\mathbf{v}^{(t_0)}, \mathbf{v}^{(t)}) = \frac{\mathbf{v}^{(t_0)} \cdot \mathbf{v}^{(t)}}{\|\mathbf{v}^{(t_0)}\| \cdot \|\mathbf{v}^{(t)}\|}, \quad (11)$$

where $\mathbf{v}^{(t_0)}$ and $\mathbf{v}^{(t)}$ are vectors composed of the sample weight of data points in S at step t_0 and step t , respectively. If the cosine similarity is smaller than the threshold γ , S will be re-selected from N_f , and the mesh will be updated.

DMIS The pseudo-code of a sampler with DMIS is shown as Algorithm 1. In each iteration, the PDE residual of data points in S are computed first, and then the sample weights of other points are estimated by interpolation. The training process combined with DMIS is shown as Figure 2.

Experiments

Benchmark

We consider to solve Schrödinger equation, Viscous Burgers' equation and Korteweg-de Vries equation. PINNs have excellent interpolation accuracy, but the extrapolation accuracy still needs to be further improved ([Kim et al. 2021](#)).

PDE	Network Config		Optimizer Config	DMIS Config			Dataset Config		
	Depth	Width	Learning rate	$ S $	γ	β	$ N_f $	$ N_i $	$ N_b $
Schrödinger	4	64	0.001	1000	0.4	2	60000	200	200
Burgers	3	32	0.005	1000	0.4	1.5	100000	2000	2000
KdV	4	64	0.001	1000	0.4	2	60000	2000	2000

Table 1: The hyper-parameters used for each benchmark. $|S|$ is the set size of mesh points, γ is the mesh update threshold, and β is the hyper-parameter of reweighting. $|N_f|$, $|N_i|$, and $|N_b|$ are the dataset size of PDE residuals, initial conditions and boundary conditions, respectively.

Method	Schrödinger Equation			Burgers' Equation			KdV Equation		
	ME	MAE	RMSE	ME	MAE	RMSE	ME	MAE	RMSE
PINN-O	1.360	0.186	0.4092	0.451	0.0738	0.1100	2.140	0.363	0.520
PINN-N	0.948	0.149	0.2906	0.358	0.0579	0.0859	1.860	0.292	0.441
xPINN	0.546	0.045	0.0089	0.261	0.0099	0.0010	2.462	0.272	0.230
cPINN	0.591	0.069	0.0169	0.324	0.0084	0.0007	2.925	0.258	0.248
PINN-DMIS(ours)	0.647	0.127	0.2196	0.225	0.0294	0.0495	1.170	0.391	0.492
xPINN-DMIS(ours)	0.867	0.036	0.0129	0.420	0.0115	0.0017	2.380	0.233	0.196
cPINN-DMIS(ours)	0.358	0.025	0.0033	0.397	0.0111	0.0016	2.680	0.230	0.200

Table 2: Comparison with PINN-O (Raissi, Perdikaris, and Karniadakis 2019), PINN-N (Nabian, Gladstone, and Meidani 2021), xPINN (Jagtap and Karniadakis 2020) and cPINN (Jagtap, Kharazmi, and Karniadakis 2020) on benchmarks of the Schrödinger Equation, the Viscous Burgers' Equation and the KdV Equation.

For this reason, the data division method used in our work is different from that in original PINNs (Raissi, Perdikaris, and Karniadakis 2019). Specifically, for each solving problem, we use the similar method as Kim et al. (2021) to divide the entire time domain $[0, T]$ into three segments: $[0, T/2]$, $[T/2, 3T/4]$ and $[3T/4, T]$. These three segments are used for training, validating, and testing.

Schrödinger Equation Schrödinger equation is a fundamental equation in quantum mechanics. Schrödinger equation with an initial condition $u(0, x) = 2sech(x)$ and periodic boundary conditions is considered:

$$i \frac{\partial u}{\partial t} + 0.5 \frac{\partial^2 u}{\partial x^2} + |u|^2 u = 0, x \in [-5, 5], t \in [0, \pi/2]. \quad (12)$$

Viscous Burgers' Equation The Burgers' equation simulates shock wave propagation and reflection. We consider the Burgers' equation with an initial condition $u(0, x) = -\sin(\pi x)$ and a boundary condition $u(t, x) = 0, x \in \{-1, 1\}$, which is shown as follows:

$$\frac{\partial u}{\partial t} + u \frac{\partial u}{\partial x} = \frac{0.04}{\pi} \frac{\partial^2 u}{\partial x^2}, x \in [-1, 1], t \in [0, 1]. \quad (13)$$

Korteweg-de Vries Equation Korteweg-de Vries (KdV) equation describes the waves on shallow water surfaces. The KdV equation, which involves third-order derivatives, is suitable to evaluate the efficiency of DMIS in solving partial differential equations with higher-order derivatives. We consider the KdV equation with an initial condition $u(0, x) = \cos(\pi x)$ and periodic boundary conditions:

$$\frac{\partial u}{\partial t} + u \frac{\partial u}{\partial x} + 0.0025 \frac{\partial^3 u}{\partial x^3} = 0, x \in [-1, 1], t \in [0, 1]. \quad (14)$$

Experimental Setting

Baseline We evaluate the performance of DMIS based on original PINN (Raissi, Perdikaris, and Karniadakis 2019), xPINN (Jagtap and Karniadakis 2020) and cPINN (Jagtap, Kharazmi, and Karniadakis 2020). The original PINN is denoted by PINN-O. PINN with importance sampling scheme of Nabian, Gladstone, and Meidani (2021) is denoted by PINN-N. PINN, xPINN and cPINN with our approach, DMIS, are denoted by PINN-DMIS, xPINN-DMIS and cPINN-DMIS, respectively.

Hyper-parameter Table 1 summarizes hyper-parameters of networks, optimizers, datasets, and DMIS for each benchmark. Collocation points are uniformly generated from the domain and domain boundary. The Adam optimizer is employed on all benchmarks. For PINN-N, we uniformly sample 10,000 seeds within the domain. For cPINN and xPINN, the spatial is equally decomposed into three subdomains.

Evaluation Metrics We choose the maximum error (ME), mean absolute error (MAE), and root mean square error (RMSE) as evaluation metrics of prediction accuracy. The exact numerical solutions are obtained by Py-PDE (Zwicker 2020). We introduce the calculation time and the number of iteration steps required for convergence, denoted by TC and NC , respectively, to evaluate the impact of sampling methods on convergence behavior. The subscript indicates the convergence level. For example, NC_5 is the minimum iteration steps required when the training loss is stable below $1e-5$ for 1000 iterations. Considering that the convergence behavior is challenging to measure, NC and TC are only used to evaluate the convergence behavior in this paper roughly. It is more intuitive to observe convergence behavior through convergence curves.

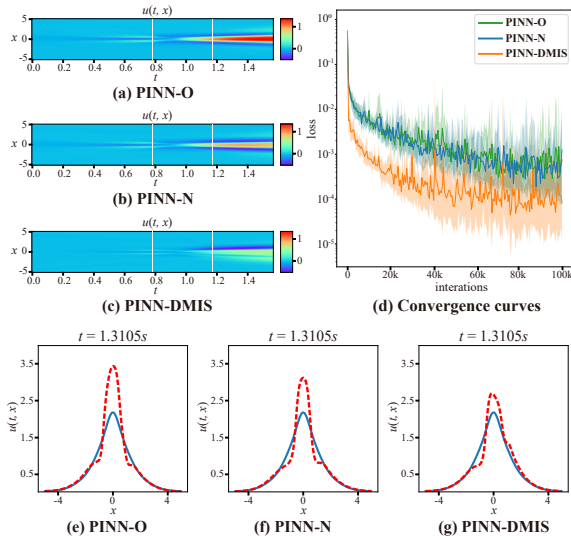


Figure 3: The Schrödinger Equation. (a, b, c) The prediction errors. (d) Convergence curves. (e, f, g) show the prediction (red) and ground-truth (blue).

	TC_2/s	TC_3/s	NC_2	NC_3
PINN-O	151	2005	4740	61984
PINN-N	466	5968	5681	72959
PINN-DMIS(ours)	34	399	847	10219

Table 3: Evaluation results of convergence behavior for solving the Schrödinger Equation

Experimental Result

Schrödinger Equation Figure 3(a, b, c) report the prediction error by PINN-O, PINN-N, and PINN-DMIS for solving Schrödinger Equation. Compared with other methods, PINN-DMIS has better performance. The snapshots in Figure 3 show that PINN-DMIS has the lowest maximum errors. Table 2 summarizes the results of prediction accuracy for solving Schrödinger Equation. DMIS can significantly improve the accuracy. Figure 3(d) reports that PINN-DMIS converges fastest and has the lowest training error. Table 3 compares the convergence behavior. PINN-DMIS shows up to five times faster convergence speed than PINN-O.

Viscous Burgers' Equation Figure 4(a, b, c) report the prediction errors for solving the Burgers' Equation. PINN-DMIS has lower prediction error in the extrapolation segment. Figure 4(e, f, g) report the snapshots of prediction at $t=0.9182s$. PINN-O and PINN-N fail to predict $u(t, x)$, and PINN-DMIS still has perfect prediction performance. Table 2 summarizes the evaluation results for solving the Viscous Burgers' Equation. PINNs-DMIS has the lowest maximum error. The convergence curves for solving the Viscous Burgers' Equation are reported in Figure 4(d). PINN-DMIS has a slender lead convergence speed. Table 4 reports the convergence behavior of PINN-O, PINN-N, and PINN-DMIS for solving the Viscous Burgers' Equation. These three methods have similar convergence behavior in the initial stage, but in

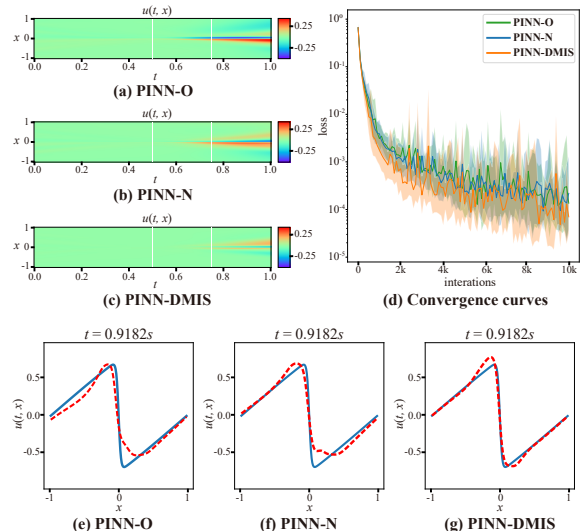


Figure 4: The Burgers' Equation. (a, b, c) The prediction errors. (d) Convergence curves. (e, f, g) show the prediction (red) and ground-truth (blue).

	TC_2/s	TC_3/s	NC_2	TC_3
PINN-O	15	97	1218	7308
PINN-N	83	417	1218	6032
PINN-DMIS(ours)	20	89	1160	5336

Table 4: Evaluation results of convergence behavior for solving the Viscous Burgers' Equation

the following stage, PINN-DMIS converges fastest.

Korteweg-de Vries Equation Figure 5(e, f, g) report the snapshots of prediction at $t=0.8347s$. all methods fail to predict $u(t, x)$. By contrast, PINN-DMIS has lower maximum error. Table 2 reports prediction accuracy and DMIS can effectively improve the accuracy of various PINNs. Figure 5(d) reports the convergence curves for solving the KdV Equation. PINN-DMIS converges faster than other methods. Table 7 reports the evaluation results of convergence behavior for solving the KdV Equation. The results indicate that PINN with DMIS has noticeable convergence acceleration.

Ablation Study

DMWE Figure 6 reports meshes constructed by DMWE and the corresponding changes of \mathcal{L} in adjacent updates. During training, mesh points gradually gather in the region with a drastic change of \mathcal{L} , and samples in these regions significantly impact the parameter optimization in the current stage. DMWE aims to arrange more mesh points in the active region to achieve a high-precision estimation of sample weight and arrange fewer mesh points in the inactive region to reduce the computational cost. The dynamic meshes shown in Figure 6 meet our expectations.

Our approach without DMWE is denoted by PINN-BasicIS. Table 5 reports evaluation results of PINN-O, PINN-BasicIS, and PINN-DMIS. Compared with PINN-

Method	Schrödinger Equation			Burgers' Equation			KdV Equation		
	ME	MAE	RMSE	ME	MAE	RMSE	ME	MAE	RMSE
PINN-O	1.360	0.186	0.409	0.451	0.074	0.110	2.140	0.363	0.520
PINN-BasicIS(ours)	0.965	0.140	0.279	0.273	0.025	0.044	1.460	0.376	0.526
PINN-DMIS(ours)	0.647	0.127	0.220	0.225	0.029	0.049	1.170	0.391	0.492

Table 5: Ablation Study of DMWE for solving the Schrödinger Equation, the Viscous Burgers' Equation and the KdV Equation.

$ S $	γ	Schrödinger Equation			Burgers' Equation			KdV Equation		
		ME	MAE	RMSE	ME	MAE	RMSE	ME	MAE	RMSE
1000	0.2	0.762	0.120	0.233	0.593	0.039	0.085	1.460	0.376	0.526
1000	0.4	0.647	0.127	0.220	0.225	0.029	0.049	1.170	0.391	0.492
1000	0.6	0.838	0.111	0.208	0.919	0.057	0.147	1.760	0.351	0.518
10000	0.4	0.913	0.132	0.262	0.392	0.033	0.075	1.280	0.366	0.475
20000	0.4	1.100	0.163	0.332	0.620	0.046	0.105	1.730	0.452	0.600

Table 6: Ablation studies of the set size $|S|$ and the mesh update threshold γ for solving the Schrödinger Equation, the Viscous Burgers' Equation and the KdV Equation.

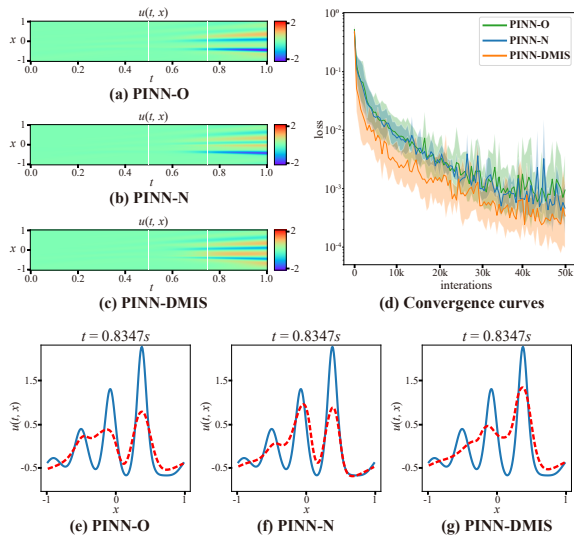


Figure 5: The KdV Equation. (a, b, c) The prediction errors. (d) Convergence curves. (e, f, g) show the prediction (red) and ground-truth (blue).

BasicIS, PINN-DMIS has better performance in most cases. Especially for solving Schrödinger Equation, PINN-DMIS has the best performance on all evaluation metrics.

Hyper-parameter Table 6 reports the ablation studies of mesh update threshold γ and set size $|S|$. When $|S|$ is too tiny, the estimation deviation of sample weights increases dramatically. On the other hand, when $|S|$ is too large, the weights of samples are unstable, which also leads to a decline of model performance. Similarly, when γ is too tiny, DMWE fails to update mesh. When γ is too large, the mesh is frequently updated, leading to a severe decrease of training efficiency. Fortunately, $\gamma = 0.4$ is always appropriate and we recommend setting γ to 0.4.

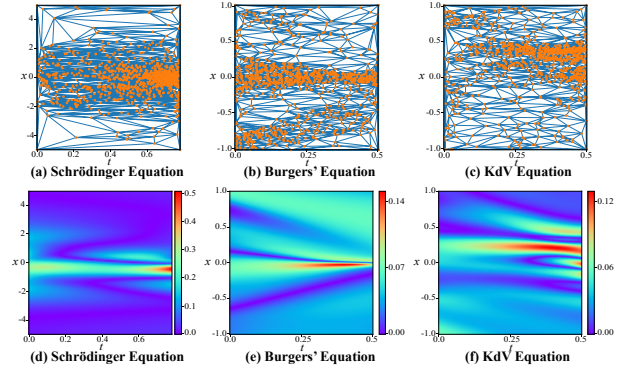


Figure 6: Dynamic mesh. (a, b, c) Meshes constructed by DMWE. (d, e, f) The corresponding changes of \mathcal{L} in adjacent updates.

	TC_2/s	TC_3/s	NC_2	NC_3
PINN-O	476	1812	12631	48401
PINN-N	794	4001	9855	49912
PINN-DMIS(ours)	288	1046	6954	25029

Table 7: Evaluation results of convergence behavior for solving the KdV Equation

Conclusion

In this paper, we propose a novel importance sampling scheme, Dynamic Mesh-based Importance Sampling (DMIS). DMIS constructs a dynamic triangular mesh to estimate sample weights and effectively integrates importance sampling into the training of PINNs. Experiments on three widely-used benchmarks show that DMIS significantly improves the convergence speed and accuracy of PINNs without significantly increasing computational cost. We also evaluate the performance of DMIS on three different PINNs models and results verify effectiveness and excellent generalization ability of DMIS.

Acknowledgments

This work is supported by the National Key Research and Development Program of China (No.2021YFB3702402) and the Scientific and Technological Innovation of Shunde Graduate School of University of Science and Technology Beijing (No. BK20AE004).

References

- Cai, W.; Li, X.; and Liu, L. 2020. A phase shift deep neural network for high frequency approximation and wave problems. *SIAM Journal on Scientific Computing*, 42(5): A3285–A3312.
- Canévet, O.; Jose, C.; and Fleuret, F. 2016. Importance sampling tree for large-scale empirical expectation. In *International Conference on Machine Learning*, 1454–1462. PMLR.
- Chen, J.; Ma, T.; and Xiao, C. 2018. FastGCN: Fast Learning with Graph Convolutional Networks via Importance Sampling. In *International Conference on Learning Representations*.
- Daw, A.; Bu, J.; Wang, S.; Perdikaris, P.; and Karpatne, A. 2022. Rethinking the Importance of Sampling in Physics-informed Neural Networks. arXiv:2207.02338.
- Dong, S.; and Ni, N. 2021. A method for representing periodic functions and enforcing exactly periodic boundary conditions with deep neural networks. *Journal of Computational Physics*, 435: 110242.
- He, K.; Zhang, X.; Ren, S.; and Sun, J. 2016. Deep residual learning for image recognition. In *Proceedings of the IEEE conference on computer vision and pattern recognition*, 770–778.
- Jagtap, A. D.; and Karniadakis, G. E. 2020. Extended Physics-Informed Neural Networks (XPINNs): A Generalized Space-Time Domain Decomposition Based Deep Learning Framework for Nonlinear Partial Differential Equations. *Communications in Computational Physics*, 28(5): 2002–2041.
- Jagtap, A. D.; Kharazmi, E.; and Karniadakis, G. E. 2020. Conservative physics-informed neural networks on discrete domains for conservation laws: Applications to forward and inverse problems. *Computer Methods in Applied Mechanics and Engineering*, 365: 113028.
- Johnson, T. B.; and Guestrin, C. 2018. Training deep models faster with robust, approximate importance sampling. *Advances in Neural Information Processing Systems*, 31.
- Kang, B.; Xie, S.; Rohrbach, M.; Yan, Z.; Gordo, A.; Feng, J.; and Kalantidis, Y. 2019. Decoupling Representation and Classifier for Long-Tailed Recognition. In *International Conference on Learning Representations*.
- Katharopoulos, A.; and Fleuret, F. 2017. Biased importance sampling for deep neural network training. arXiv:1706.00043.
- Katharopoulos, A.; and Fleuret, F. 2018. Not all samples are created equal: Deep learning with importance sampling. In *International Conference on Machine Learning*, 2525–2534. PMLR.
- Kim, J.; Lee, K.; Lee, D.; Jhin, S. Y.; and Park, N. 2021. DPM: a novel training method for physics-informed neural networks in extrapolation. In *Proceedings of the AAAI Conference on Artificial Intelligence*.
- Krishnapriyan, A.; Gholami, A.; Zhe, S.; Kirby, R.; and Mahoney, M. W. 2021. Characterizing possible failure modes in physics-informed neural networks. In *Advances in Neural Information Processing Systems*, 26548–26560.
- Krizhevsky, A.; Sutskever, I.; and Hinton, G. E. 2012. ImageNet classification with deep convolutional neural networks. In *Advances in Neural Information Processing Systems*.
- Lei, J.; Li, L.; Zhou, L.; Gan, Z.; Berg, T. L.; Bansal, M.; and Liu, J. 2021. Less is more: Clipbert for video-and-language learning via sparse sampling. In *Proceedings of the IEEE/CVF Conference on Computer Vision and Pattern Recognition*, 7331–7341.
- Loshchilov, I.; and Hutter, F. 2015. Online batch selection for faster training of neural networks. arXiv:1511.06343.
- Lu, L.; Meng, X.; Mao, Z.; and Karniadakis, G. E. 2021. DeepXDE: A deep learning library for solving differential equations. *SIAM Review*, 63(1): 208–228.
- Meng, C.; Liu, E.; Neiswanger, W.; Song, J.; Burke, M.; Lobell, D.; and Ermon, S. 2022. IS-COUNT: Large-scale Object Counting from Satellite Images with Covariate-based Importance Sampling. In *Proceedings of the AAAI Conference on Artificial Intelligence*, 12034–12042.
- Meng, X.; Li, Z.; Zhang, D.; and Karniadakis, G. E. 2020. PPINN: Parareal physics-informed neural network for time-dependent PDEs. *Computer Methods in Applied Mechanics and Engineering*, 370: 113250.
- Mildenhall, B.; Srinivasan, P.; Tancik, M.; Barron, J.; Ramamoorthi, R.; and Ng, R. 2020. Nerf: Representing scenes as neural radiance fields for view synthesis. In *European conference on computer vision*.
- Nabian, M. A.; Gladstone, R. J.; and Meidani, H. 2021. Efficient training of physics-informed neural networks via importance sampling. *Computer-Aided Civil and Infrastructure Engineering*, 36(8): 962–977.
- Needell, D.; Ward, R.; and Srebro, N. 2014. Stochastic gradient descent, weighted sampling, and the randomized Kaczmarz algorithm. In *Advances in Neural Information Processing Systems*.
- Niaki, S. A.; Haghghat, E.; Campbell, T.; Poursartip, A.; and Vaziri, R. 2021. Physics-informed neural network for modelling the thermochemical curing process of composite-tool systems during manufacture. *Computer Methods in Applied Mechanics and Engineering*, 384: 113959.
- Pang, G.; Lu, L.; and Karniadakis, G. E. 2019. fPINNs: Fractional physics-informed neural networks. *SIAM Journal on Scientific Computing*, 41(4): A2603–A2626.
- Qiu, Z.; Qiu, K.; Fu, J.; and Fu, D. 2019. Learning recurrent structure-guided attention network for multi-person pose estimation. In *2019 IEEE International Conference on Multi-media and Expo (ICME)*, 418–423. IEEE.

Qiu, Z.; Qiu, K.; Fu, J.; and Fu, D. 2020. Dgcn: Dynamic graph convolutional network for efficient multi-person pose estimation. In *Proceedings of the AAAI Conference on Artificial Intelligence*, 11924–11931.

Qiu, Z.; Yang, Q.; Wang, J.; and Fu, D. 2022. Dynamic Graph Reasoning for Multi-person 3D Pose Estimation. In *Proceedings of the 30th ACM International Conference on Multimedia*, 3521–3529.

Raissi, M.; Perdikaris, P.; and Karniadakis, G. E. 2019. Physics-informed neural networks: A deep learning framework for solving forward and inverse problems involving nonlinear partial differential equations. *Journal of Computational Physics*, 378: 686–707.

Raissi, M.; Yazdani, A.; and Karniadakis, G. E. 2020. Hidden fluid mechanics: Learning velocity and pressure fields from flow visualizations. *Science*, 367(6481): 1026–1030.

Schaul, T.; Quan, J.; Antonoglou, I.; and Silver, D. 2015. Prioritized experience replay. arXiv:1511.05952.

Shrivastava, A.; Gupta, A.; and Girshick, R. 2016. Training region-based object detectors with online hard example mining. In *Proceedings of the IEEE conference on computer vision and pattern recognition*, 761–769.

Sirignano, J.; and Spiliopoulos, K. 2018. DGM: A deep learning algorithm for solving partial differential equations. *Journal of Computational Physics*, 375: 1339–1364.

Umetani, N.; and Bickel, B. 2018. Learning three-dimensional flow for interactive aerodynamic design. *ACM Transactions on Graphics*, 37(4): 1–10.

Wandel, N.; Weinmann, M.; Neidlin, M.; and Klein, R. 2022. Spline-pinn: Approaching pdes without data using fast, physics-informed hermite-spline cnns. In *Proceedings of the AAAI Conference on Artificial Intelligence*.

Wang, S.; Teng, Y.; and Perdikaris, P. 2021. Understanding and mitigating gradient flow pathologies in physics-informed neural networks. *SIAM Journal on Scientific Computing*, 43(5): A3055–A3081.

Wang, S.; Yu, X.; and Perdikaris, P. 2022. When and why PINNs fail to train: A neural tangent kernel perspective. *Journal of Computational Physics*, 449: 110768.

Wang, Y.; Xu, C.; Du, B.; and Lee, H. 2021. Learning to weight imperfect demonstrations. In *International Conference on Machine Learning*, 10961–10970. PMLR.

Wu, C.; Zhu, M.; Tan, Q.; Kartha, Y.; and Lu, L. 2022. A comprehensive study of non-adaptive and residual-based adaptive sampling for physics-informed neural networks. arXiv:2207.10289.

Zhang, D.; Guo, L.; and Karniadakis, G. E. 2020. Learning in modal space: Solving time-dependent stochastic PDEs using physics-informed neural networks. *SIAM Journal on Scientific Computing*, 42(2): A639–A665.

Zhao, P.; and Zhang, T. 2015. Stochastic optimization with importance sampling for regularized loss minimization. In *international Conference on Machine Learning*.

Zwicker, D. 2020. py-pde: A python package for solving partial differential equations. *Journal of Open Source Software*, 5(48): 2158.

Appendix A: Supporting Theory

In this section, we supplement some deductions.

Exact Importance Sampling for Neural Networks

Parameters of neural networks are optimized by training. The goal of training is as follows.

$$\begin{aligned}\boldsymbol{\theta}^* &= \arg \min_{\boldsymbol{\theta}} \mathcal{L}, \\ &= \arg \min_{\boldsymbol{\theta}} \frac{1}{|N|} \sum_{\mathbf{x} \in N} \ell(\mathbf{x}; \boldsymbol{\theta}),\end{aligned}\quad (15)$$

where N is a dataset, \mathbf{x} is a data point in N , $\boldsymbol{\theta}$ is parameters of neural networks, $\boldsymbol{\theta}^*$ is the optimal parameters, ℓ is a loss function, and \mathcal{L} is the total loss.

Parameters of neural networks are updated according to the gradient of \mathcal{L} :

$$\begin{aligned}\boldsymbol{\theta}^{(t+1)} &= \boldsymbol{\theta}^{(t)} - \eta \nabla_{\boldsymbol{\theta}^{(t)}} \mathcal{L}, \\ &= \boldsymbol{\theta}^{(t)} - \eta \nabla_{\boldsymbol{\theta}^{(t)}} \frac{1}{|N|} \sum_{\mathbf{x} \in N} \alpha_{\mathbf{x}} \ell(\mathbf{x}; \boldsymbol{\theta}),\end{aligned}\quad (16)$$

where $\alpha_{\mathbf{x}}$ is a sample weight, $\boldsymbol{\theta}^{(t)}$ and $\boldsymbol{\theta}^{(t+1)}$ are parameters at iterations t and $t+1$, respectively, and η is learning rate. For uniform sampling, $\alpha_{\mathbf{x}} = 1$. Assuming that the sampling probability of \mathbf{x} is $q_{\mathbf{x}}$, with the condition of unbiased estimation, the sample weight $\alpha_{\mathbf{x}} = 1/(|N|q_{\mathbf{x}})$. We aim to find the best sampling probability $q_{\mathbf{x}}$ to make the training convergence rate fastest.

In our paper, the convergence rate of training is defined as follows (Needell, Ward, and Srebro 2014; Zhao and Zhang 2015).

$$C^{(t)} = -\mathbb{E}[\|\boldsymbol{\theta}^{(t+1)} - \boldsymbol{\theta}^*\|_2^2 - \|\boldsymbol{\theta}^{(t)} - \boldsymbol{\theta}^*\|_2^2], \quad (17)$$

where $C^{(t)}$ is the convergence rate at iteration t , and \mathbb{E} denotes expectation.

For the convenience of subsequent discussion, We set $G^{(t)} = \eta \nabla_{\boldsymbol{\theta}^{(t)}} \mathcal{L}$, $D^{(t)} = \|\boldsymbol{\theta}^{(t)} - \boldsymbol{\theta}^*\|_2^2$, and $D^{(t)} = \|\boldsymbol{\theta}^{(t)} - \boldsymbol{\theta}^*\|_2^2$.

$D^{(t)}$ and $D^{(t+1)}$ can be simplified as follows.

$$\begin{aligned}D^{(t)} &= (\boldsymbol{\theta}^{(t)} - \boldsymbol{\theta}^*)^T (\boldsymbol{\theta}^{(t)} - \boldsymbol{\theta}^*), \\ &= \|\boldsymbol{\theta}^{(t)}\|_2^2 - 2\boldsymbol{\theta}^{(t)T} \boldsymbol{\theta}^* + \|\boldsymbol{\theta}^*\|_2^2.\end{aligned}\quad (18)$$

$$\begin{aligned}D^{(t+1)} &= (\boldsymbol{\theta}^{(t+1)} - \boldsymbol{\theta}^*)^T (\boldsymbol{\theta}^{(t+1)} - \boldsymbol{\theta}^*), \\ &= \|\boldsymbol{\theta}^{(t+1)}\|_2^2 - 2\boldsymbol{\theta}^{(t+1)T} \boldsymbol{\theta}^* + \|\boldsymbol{\theta}^*\|_2^2, \\ &= \|\boldsymbol{\theta}^{(t)} - \eta G^{(t)}\|_2^2 - 2(\boldsymbol{\theta}^{(t)} - \eta G^{(t)})^T \boldsymbol{\theta}^* + \|\boldsymbol{\theta}^*\|_2^2.\end{aligned}\quad (19)$$

According to Equation (18) and (19), the convergence rate can be simplified as follows.

$$\begin{aligned}C^{(t)} &= -\mathbb{E}[D^{(t+1)} - D^{(t)}], \\ &= -\mathbb{E}[\|\boldsymbol{\theta}^{(t)} - \eta G^{(t)}\|_2^2 + 2\eta G^{(t)T} \boldsymbol{\theta}^* - \|\boldsymbol{\theta}^{(t)}\|_2^2], \\ &= -\mathbb{E}[-2\eta(\boldsymbol{\theta}^{(t)} - \boldsymbol{\theta}^*)G^{(t)} + \eta^2 G^{(t)T} G^{(t)}], \\ &= 2\eta(\boldsymbol{\theta}^{(t)} - \boldsymbol{\theta}^*)\mathbb{E}[G^{(t)}] - \eta^2 \mathbb{E}[G^{(t)}]^T \mathbb{E}[G^{(t)}], \\ &\quad - \eta^2 \text{Tr}(\mathbb{V}[G^{(t)}]),\end{aligned}\quad (20)$$

where Tr denotes trace, and \mathbb{V} denotes variance.

The expectation of the gradient is independent of the sampling probability $p_{\mathbf{x}}$. maximizing convergence rate is equivalent to minimize $\text{Tr}(\mathbb{V}[G^{(t)}])$, and Needell, Ward, and Srebro (2014); Zhao and Zhang (2015) have demonstrated that the best sampling distribution is determined by $q_{\mathbf{x}}^{(t)*} \propto \|\nabla_{\boldsymbol{\theta}^{(t)}} \ell(\mathbf{x}, \boldsymbol{\theta}^{(t)})\|_2$.

Optimization Problem of PINNs

As mentioned in the main content, PINNs learn approximate solutions $\hat{u}(t, \mathbf{x}; \boldsymbol{\theta})$ to fit the latent solutions $u(t, \mathbf{x})$ of PDEs.

$$\begin{aligned}\frac{\partial u}{\partial t} + \mathcal{N}_{\mathbf{x}}[u] &= 0, \mathbf{x} \in \Omega, t \in [0, T], \\ u(t, \mathbf{x})|_{t=0} &= u_0(\mathbf{x}), \mathbf{x} \in \Omega, \\ u(t, \mathbf{x}) &= g(t, \mathbf{x}), \mathbf{x} \in \partial\Omega, t \in [0, T],\end{aligned}\quad (21)$$

where $\boldsymbol{\theta}$ is the parameter of PINNs, $\mathcal{N}_{\mathbf{x}}$ denotes a differential operator consisted of spatial derivatives, $u_0(\mathbf{x})$ is the initial condition, $g(\mathbf{x})$ is the boundary condition, \mathbf{x} is a D-dimensional position vector, and Ω is a subset of \mathbb{R}^D with boundary $\partial\Omega$.

PINNs regard boundary conditions and initial conditions as penalty terms and formulate the constrained optimization problem into an unconstrained optimization problem:

$$\boldsymbol{\theta}^* = \arg \min_{\boldsymbol{\theta}} r_f(\boldsymbol{\theta}) + \lambda_1 r_i(\boldsymbol{\theta}) + \lambda_2 r_b(\boldsymbol{\theta}), \quad (22)$$

where λ_1 and λ_2 are weights, $r_f(\boldsymbol{\theta})$, $r_i(\boldsymbol{\theta})$ and $r_b(\boldsymbol{\theta})$ are the residuals of PDEs, initial conditions, and boundary conditions, respectively.

The residual of PDEs is an integral over the spatial-temporal domain:

$$r_f(\boldsymbol{\theta}) = \int_{\Omega \times [0, T]} \left(\frac{\partial \hat{u}}{\partial t} + \mathcal{N}_{\mathbf{x}}[\hat{u}] \right)^2 d\mathbf{x} dt. \quad (23)$$

The residual of initial conditions is an integral over the spatial domain with $t = 0$:

$$r_i(\boldsymbol{\theta}) = \int_{\Omega} (\hat{u}(0, \mathbf{x}) - u_0(\mathbf{x}))^2 d\mathbf{x}. \quad (24)$$

The residual of boundary conditions is an integral over the boundary of domain:

$$r_b(\boldsymbol{\theta}) = \int_{\partial\Omega \times [0, T]} (\hat{u}(t, \mathbf{x}) - g(t, \mathbf{x}))^2 d\mathbf{x} dt. \quad (25)$$

Equation 22 can be approximated as a loss function of data points:

$$\begin{aligned}\boldsymbol{\theta}^* &\approx \arg \min_{\boldsymbol{\theta}} \mathcal{L}, \\ &= \arg \min_{\boldsymbol{\theta}} \mathcal{L}_f + \lambda_1 \mathcal{L}_i + \lambda_2 \mathcal{L}_b,\end{aligned}\quad (26)$$

where \mathcal{L} is the total loss, \mathcal{L}_f , \mathcal{L}_i , and \mathcal{L}_b are the losses of PDE residuals, initial conditions, and boundary conditions, respectively. The datasets of these losses are denoted by N_f , N_i and N_b , respectively.

$$\begin{aligned}
\mathcal{L}_f &= \frac{1}{|N_f|} \sum_{\mathbf{x} \in N_f} \ell_f(\mathbf{x}; \boldsymbol{\theta}), \\
&= \frac{1}{|N_f|} \sum_{i=1}^{|N_f|} \left\| \frac{\partial \hat{u}}{\partial t_i} + \mathcal{N}_{\mathbf{x}_i} [\hat{u}(t_i, \mathbf{x}_i)] \right\|_2^2,
\end{aligned} \tag{27}$$

where ℓ_f is the loss of a data point $\mathbf{x} \in N_f$.

$$\begin{aligned}
\mathcal{L}_i &= \frac{1}{|N_i|} \sum_{\mathbf{x} \in N_i} \ell_i(\mathbf{x}; \boldsymbol{\theta}), \\
&= \frac{1}{|N_i|} \sum_{i=1}^{|N_i|} \|\hat{u}(t_i, \mathbf{x}_i) - g(t_i, \mathbf{x}_i)\|_2^2,
\end{aligned} \tag{28}$$

where ℓ_i is the loss of a data point $\mathbf{x} \in N_i$.

$$\begin{aligned}
\mathcal{L}_b &= \frac{1}{|N_b|} \sum_{\mathbf{x} \in N_b} \ell_b(\mathbf{x}; \boldsymbol{\theta}), \\
&= \frac{1}{|N_b|} \sum_{i=1}^{|N_b|} \|\hat{u}(0, \mathbf{x}_i) - u_0(\mathbf{x}_i)\|_2^2,
\end{aligned} \tag{29}$$

where ℓ_b is the loss of a data point $\mathbf{x} \in N_b$.

In DMIS, importance sampling is integrated into the training, and the detail of DMIS is described in the main content.

Appendix C: Additional Experiment

In this section, we supplement the experiments of solving the Diffusion Equation and the Allen-Cahn (AC) equation.

Benchmark

The same method has been used as described in the main content to divide the entire time domain $[0, T]$ into three segments: $[0, T/2]$, $[T/2, 3T/4]$, and $[3T/4, T]$. These three segments are used for training, validating, and testing.

Diffusion Equation The diffusion equation is a crucial partial differential equation used to describe the change of matter density in the diffusion phenomenon. This equation can also describe the heat conduction process. We consider the diffusion equation with an initial condition $u(0, x) = 2\sin(\pi x) + 2x - 2x^3$ and a boundary condition $u(t, x) = 0, x \in \{0, 1\}$.

$$\frac{\partial u}{\partial t} = 1.2 \frac{\partial^2 u}{\partial x^2} + 5e^{-t}x, x \in [0, 1], t \in [0, 1]. \tag{30}$$

Allen-Cahn Equation The Allen-Cahn (AC) equation is a type of reaction-diffusion equation. This equation is also the main mathematical model for phase-field simulation in material science, which describes the phase separation process of multi-component alloys. We consider the AC equation with an initial condition $u(0, x) = x^2 \cos(\pi x)$ and periodic boundary conditions:

$$\frac{\partial u}{\partial t} = \frac{0.001}{\pi} \frac{\partial^2 u}{\partial x^2} + 2\sin(\pi u), x \in [-1, 1], t \in [0, 1]. \tag{31}$$

Experimental Setting

Hyper-parameter Table 8 summarizes hyper-parameters for each additional benchmark. The Adam optimizer is used on all additional benchmarks. For PINN-N, we uniformly sample 10,000 seeds within the domain, and other parameters are consistent with Table 8. Experiments on each additional benchmark have same random seed.

Evaluation Metrics We use the same evaluation metrics as described in the main content. The maximum error(AE), mean absolute error (MAE), and root mean square error (RMSE) are used to evaluate prediction accuracy. The calculation time TC and the number of iteration steps NC required for convergence are used to evaluate convergence behavior.

Experimental Result

Diffusion Equation Figure 7(a, b, c) report the prediction error by PINN-O, PINN-N, and PINN-DMIS for solving the diffusion equation. Compared with other state-of-the-art methods, DMIS has best performance. The snapshots in Figure 7 show that DMIS has the best prediction results in the whole domain. Table 9 summarizes the evaluation results of prediction accuracy for solving Diffusion Equation. DMIS has the best performance on all evaluation metrics. Figure 7(d) reports the convergence curves for solving the Diffusion Equation. DMIS converges fastest and has the lowest training error. However, the loss value fluctuates greatly in DMIS. We speculate that the loss value fluctuates greatly due to the unstable sample weights. Affected by the complex initial conditions, the triangular mesh updates frequently during training. Table 10 compares the convergence behaviors. DMIS has the fastest convergence speed.

Allen-Cahn Equation Figure 8(a, b, c) report the prediction errors for solving the Allen-Cahn Equation. DMIS has the lowest prediction error. Figure 8(e, f, g) report the snapshots of prediction at $t=0.8347s$. Compared with PINN-O and PINN-N, DMIS has better prediction results on the position with large gradient. Table 9 summarizes the evaluation results for solving the Allen-Cahn Equation. DMIS has the best performance on all evaluation metrics. The convergence curves for solving the Allen-Cahn Equation are reported in Figure 8(d). DMIS does not show obvious advantages. The result shows that DMWE fails to generate an effective mesh. The failure reason are analyzed in detail in next section. Table 11 reports the convergence behaviors for solving the Allen-Cahn Equation. These three methods have similar convergence behavior and DMIS has a slender lead convergence speed.

Appendix D: Limitations of DMIS

Because DMIS is based on importance sampling, when importance sampling fails, DMIS also fails to speed up the training of PINNs. If all data points have the same loss value, the sampling probabilities of data points are equal to $1/|N_f|$, and the importance sampling degenerates into uniform sampling. In this case, DMIS is not only unable to accelerate training, but also causes additional computational costs.

PDE	Network Config		Optimizer Config	DMIS Config			Dataset Config		
	Depth	Width	Learning rate	$ S $	γ	β	$ N_f $	$ N_i $	$ N_b $
Diffusion	4	32	0.002	1000	0.4	2	100000	2000	2000
Allen-Cahn	5	64	0.001	1000	0.4	1.5	60000	2000	2000

Table 8: The hyper-parameters used for each benchmark. $|S|$ is the set size of mesh points, γ is the mesh update threshold, and β is the hyper-parameter of reweighting. $|N_f|$, $|N_i|$, and $|N_b|$ are the dataset size of PDE residuals, initial conditions and boundary conditions, respectively.

Method	Diffusion Equation			Allen-Cahn Equation		
	ME	MAE	RMSE	ME	MAE	RMSE
PINN-O	0.181	0.089	0.095	1.406	0.133	0.232
PINN-N	0.158	0.076	0.081	1.404	0.107	0.203
PINN-DMIS(ours)	0.053	0.016	0.019	1.037	0.086	0.150

Table 9: Comparison with PINN-O (Raissi, Perdikaris, and Karniadakis 2019) and PINN-N (Nabian, Gladstone, and Meidani 2021) on benchmarks of the Diffusion Equation and the Allen-Cahn Equation.

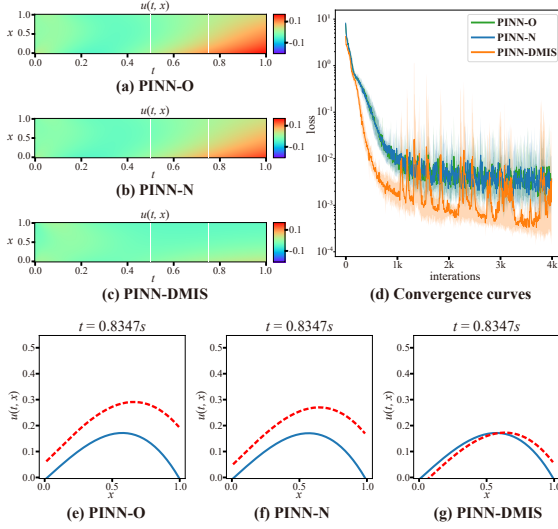


Figure 7: The Diffusion Equation. (a, b, c) The prediction errors of PINN-O, PINN-N and PINN-DMIS, respectively. (d) Convergence curves. (e, f, g) show the prediction (red) and ground-truth (blue).

	TC_1/s	TC_2/s	NC_1	NC_2
PINN-O	19	42	1089	2420
PINN-N	82	173	1089	2299
PINN-DMIS(ours)	18	21	847	968

Table 10: Evaluation results of convergence behavior for solving the Diffusion Equation

In practice, considering the loss values of data points are not precisely equal, DMIS is always valid. However, we still need to pay attention to the balance between the improvement and the additional calculation cost brought by DMIS. In our experiments, DMIS shows excellent performance in solving the Schrödinger equation. In solving the Schrödinger equation, DMIS can significantly improve the convergence efficiency because the loss values of data points are quite different. On the other hand, in solving the Allen-

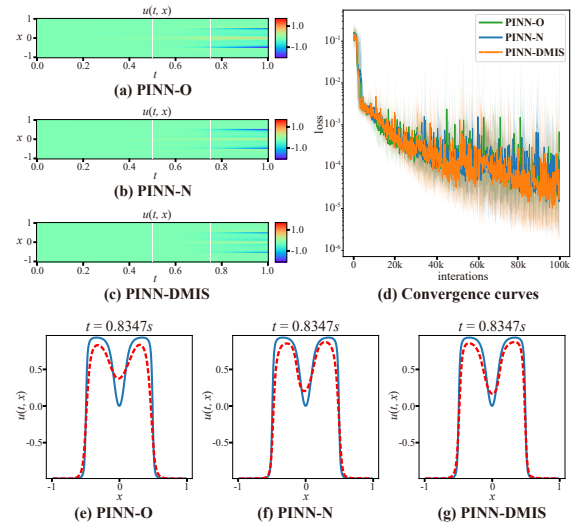


Figure 8: The Allen-Cahn Equation. (a, b, c) The prediction errors of PINN-O, PINN-N and PINN-DMIS, respectively. (d) Convergence curves. (e, f, g) show the prediction (red) and ground-truth (blue).

	TC_1/s	TC_2/s	NC_1	NC_2
PINN-O	70	97	2847	3989
PINN-N	213	304	3181	4562
PINN-DMIS(ours)	67	104	2243	3459

Table 11: Evaluation results of convergence behavior for solving the Allen-Cahn Equation

Cahn equation, DMIS almost degenerates into uniform sampling.

In addition to the limitation brought by importance sampling, the triangular mesh also affects the effect of DMIS. For DMIS, the instability of the loss value distribution leads to frequent updating of the triangular mesh, which affects the training efficiency and the stability of training. In solving the diffusion equation, the mesh updates frequently, and the loss value fluctuates greatly, as shown in Figure 7(d).

These defects can be alleviated by setting an appropriate updating threshold. The selection of the threshold mainly depends on experience. Fortunately, our experiments show that the impact of threshold is relatively stable within a reasonable range $[0.3, 0.6]$ and we recommend setting the threshold γ to 0.4.

In this paper, we only verify the excellent performance and generalization ability of DMIS on five widely-used benchmarks. We will verify the applicability of DMIS on more complex PDEs, for example high-dimensional PDEs, in the future.